Weakened El Niño Predictability in the Early 21st Century

Mei Zhao[1], Harry H. Hendon[1], Oscar Alves[1], Guo Liu[1], Guomin Wang[1]

[1]Bureau of Meteorology
Docklands, Australia 3008

Predictive skill for El Nino-Southern Oscillation (ENSO) during 2000-2013 declined sharply relative to that achieved during 1980-1999[1] despite improvements of forecast systems[2,3] and initial conditions[4,5]. This decline in skill coincides with a reduction of ENSO activity[6] and a shift in Pacific climate to a stronger Walker circulation[7,8,9], which has previously been associated with the recent pause in global-mean surface warming[10,11]. We show using seasonal forecast sensitivity experiments that this shift in Pacific climate also drove the drop in ENSO predictive skill because the atmosphere-ocean feedbacks that sustain ENSO are weakened. Weakened atmosphere-ocean coupling due to the ongoing strengthened Walker circulation helps explain the unpredictable behaviour of El Niño in 2014. The recent decadal decline in ENSO predictability is a sobering reminder that the long lead prediction achieved during 1980-1999 might not be achievable in the future, although the robust impacts of the background Pacific climate variation on ENSO predictability indicate the potential for prediction of decadal variations in ENSO activity. However, anticipating future changes in ENSO predictability poses challenges because the causes and predictability of the change in background tropical Pacific climate, including any contribution of anthropogenic climate change, are as yet poorly quantified and simulated[11,12,13].

ENSO causes major changes to rainfall, temperature, and severe weather in many parts of the world, with impacts on agricultural production, water resources, and ecosystems[14]. Fortunately, the occurrence of ENSO can be predicted up to 2-3 seasons in advance[14], which helps in preparing for ENSO-driven impacts. Hence, unravelling the decline in ENSO predictive skill in the early 21st century, which has been reported across a range of dynamical and statistical forecast systems[1], is important to guide future development of prediction systems and to inform the level of climate predictability that might be achieved in the future. This recent decline in ENSO prediction skill is demonstrated by comparing hindcast predictions (referred to as control forecasts) of surface temperature in the equatorial eastern Pacific during 2000-2013 and 1981-1999 using the Australian Bureau of Meteorology operational seasonal forecast system[4] (Fig. 1d): the level of skill that was achievable to 9 months lead time in the late 20th century is only be attained to 3 month lead in the early 21st century. The further drop in skill when 2000-2013 is compared to 2000-2010 indicates that the previously reported decline in skill for the early 2000's is ongoing.

This dramatic drop in forecast skill in the recent two decades coincides with a marked reduction in ENSO activity[6] as indicated by reduced temperature variability in the Niño3 region (Fig. 1a). The drop in forecast skill thus can be understood as resulting from decreased signal-to-noise: big events are easier to predict than weak events[1,15,16]. This impact of variability on predictive skill is demonstrated by a decrease in forecast skill when the two large El Niño episodes in 1982/83 and 1997/98 are excluded from the assessment of skill in the earlier epoch by comparing 1981-1999 to 1985-1995 (Fig. 1d).

The reduction of ENSO activity, which can explain the drop in forecast skill in the early 21st century, has been postulated to result from a random reduction in ENSO events'[17]. However, the recharge-discharge mechanism that provides the long lead predictability of ENSO[14] also weakened in the recent epoch[18], which indicates that there have been changes in the primary mechanism causing ENSO that might have contributed to the decline in forecast skill.

Concurrent with the decline in ENSO variability and predictive skill, the climate of the Pacific varied decadally as manifest by a swing in the Interdecadal Pacific Oscillation (IPO) to its cold phase after the strong El Niño 1997-98[7,8,8,10,11,17]. The key changes in background climate are captured by the epochal mean differences shown in Figs. 1a,b,c. The recent epoch is characterized by stronger trade winds in the central and western Pacific, a strengthened east-west surface temperature gradient, westward displaced equatorial upwelling, and a more steeply tilted thermocline[6]. The upwelling change reflects the local response to changes in surface stress, whereas the steepened thermocline stems from the integrated effect of increased trade winds across the basin. The increased trade winds are reflective of a stronger Walker Circulation[97,8,9,10,11] with increased rainfall and lower surface pressure over a warmer western Pacific and Indian Oceans and reduced rainfall, higher pressure and stronger subsidence over a colder eastern Pacific (Supplementary Fig. 1). This shift in background climate is counter to that anticipated by anthropogenic climate change[12] and has been associated with the recent hiatus in global warming[10,11], but here we will show it has also acted to reduce ENSO variability and predictability and so results in lower predictive skill.

We demonstrate this with a forecast sensitivity experiment, whereby we re-run the seasonal hindcasts in the later epoch but initialized with the background climate from the earlier epoch, and vice versa for the hindcasts in the earlier epoch (see Methods). We then compare ENSO prediction between pairs of control and experiment hindcasts. The strength of this approach is that rather than assessing impacts of projected or idealized variations of background climate on ENSO evolution[162,13,19,20], observed background changes are imposed onto observed initial anomalies using a forecast model whose past performance for predicting the observed ENSO is established[4]. Any detected changes in ENSO predictability thus should reflect impacts of the observed changes in background climate. This approach also removes the ambiguity of whether the enhanced predictability in the earlier epoch was simply due to the random occurrence of stronger ENSO events then because by design we assess the impact of the mean state change on the events that did occur in each epoch.

Initializing the forecasts in the later epoch with the background climate from the earlier epoch results in increased ENSO amplitude (Fig. 2a) and predictability (Fig. 2b), and vice versa for the forecasts in the earlier epoch. The differences grow with lead time, and by 6 months the changes in amplitude are comparable to the observed differences between the two epochs (compare Supplementary Figs. 4c,f to Fig. 1a). Predictability differences are comparable to the epochal differences in the control forecasts (Fig. 2b), with the biggest changes occurring for forecasts initialized in the first half of the year (Supplementary Fig. 5) when ENSO is most rapidly growing. Importantly, the initial mean state changes are largely maintained through the first few months of the experiment similar to the epochal differences in the control forecasts (Supplementary Figs. 2a-c), so we are confident that detected changes in ENSO behaviour stem from the imposed initial differences in background climate.

The impact of the background climate change on individual El Nino and La Nina events is demonstrated by the scatter of the differences in predicted Niño3 index at 1 month lead versus the observed Niño3 index anomaly at the initial time (Figs. 3 c and d), recalling that the control and experiment forecasts are initialized with the same observed Nino3 anomaly. Importantly, El Niños get warmer and La Niñas get colder in the presence of the background climate from the earlier epoch (and vice versa in response to background climate in the later epoch), confirming that the mechanisms causing ENSO are altered by the change in background climate. The slope of the regression in Figs. 3c,d, which has nearly identical magnitude but opposite sign in the two epochs, is interpreted as the difference in growth rate of an ENSO anomaly in response to the change in background climate (see Methods) and has magnitude of about 15% of the typical ENSO growth rate. This regression is also computed at every model grid point (Fig, 3 a,b) and shows that the difference in growth rate has largest amplitude in the equatorial eastern Pacific where ENSO variability is strongest and the pattern is similar to the observed epochal changes in variability (Fig. 1a) and predicted differences in amplitude (Supplementary Fig. 4).

Positive feedbacks involving the atmosphere and ocean are fundamental to development of ENSO[14,21]: the ENSO ocean surface temperature anomaly drives rainfall and zonal wind variations that act to strengthen the ocean temperature anomaly[21]. The strength of these feedbacks depends on the background climate[14]. The difference (experiment minus control) heat budget in the upper ocean (Supplementary Information) reveals how these feedbacks respond to changes in the background climate (Supplementary Fig. 6). Reduced ENSO variability during the recent epoch results from a roughly equal contribution of weakened "thermocline feedback" (i.e., the growth of a temperature anomaly due to advection of thermocline perturbations by mean upwelling) because of reduced mean upwelling east of the dateline (Fig. 1c), and weakened "zonal advective feedback" (ie growth of temperature anomaly due to advection of the mean zonal SST gradient by anomalous zonal currents; Supplementary Fig. 6d) because of weaker generated zonal current anomalies in the central Pacific[7,9]. An increase of zonal advective feedback in the far western Pacific, due to the intensified surface temperature gradient in the recent epoch (Fig. 1a), is also detected (Supplementary Fig. 6c) and has been attributed to be the cause of the recent increase of surface temperature variability in the western Pacific[7,9,20].

Weakened zonal advective feedback in the central Pacific during the recent epoch stems from weakened atmosphere-ocean coupling[7,9,20]: based on observed data, the westerly (easterly) wind response to an El Niño (La Niña) surface temperature anomaly is shifted west in the recent epoch (Supplementary Fig. 7), which results in a weaker ocean response to the east[7,9]. This change in the zonal wind response comes about because a) a surface temperature anomaly developing in the colder eastern Pacific during the recent epoch will produce a weaker and westward shifted rainfall response[7,9,19,20] and b) stronger mean subsidence in the eastern Pacific in the recent epoch due to the strengthened Walker circulation acts to suppress the rainfall/wind response to a surface temperature anomaly[7,9].

These findings shed light onto the challenges of predicting development of El Niño in early 2014, which stalled during boreal summer after strong development during spring[22]. Forecasts from initial conditions on 1 April 2014 (Fig. 4a) predicted continued development of El Niño but underestimated the decay around July, which has been attributed to the lack of an accompanying sustained response in the atmosphere as embodied by a negative swing in the Southern Oscillation[22]. Forecasts from 1 May 2014 (Fig. 4b) well captured the demise in July but now predict near-neutral conditions by year's end. In contrast, if these forecasts are remade using the background climate from the late 20th century, a much stronger, more predictable El Niño develops from 1 April, while little decay is predicted from 1 May, suggesting that the fickle nature of El Niño 2014 reflects weakened atmosphere-ocean coupling as a result of the ongoing shift in background climate.

The robust impact of variations in background Pacific climate on ENSO activity and predictability suggest the potential for prediction of decadal variations in ENSO activity. However, we have not provided insight as to what caused the recent intensification of the Walker circulation. It might stem from natural, yet largely unpredictable, decadal variations of Pacific climate[13,19,20,23], or it may be a response to forced climate change such that the eastern Pacific warms more slowly than the other oceans[24,25]. Furthermore, although a consensus is emerging about expected changes of ENSO impacts in a warming climate[26], there is as yet little insight or as to how ENSO predictability might change because there is little agreement as to how ENSO activity might change[12]. The recent shift in Pacific climate appears to be not well simulated with contemporary climate models[11], suggesting model errors are limiting the capability to simulate and predict variations of Pacific climate that are relevant to future variations of ENSO activity. We suggest that our approach of evaluating ensembles of short-lead seasonal predictions, initialized from observed states at multiple start times from different climate epochs could be an efficient manner to reveal the source of error in the representation of climate variations such as those discussed here, and so lead to improved climate models that are of more utility for predicting future climate.

Methods

Coupled Model Seasonal Hindcasts

A 10-member ensemble of 9-month control hindcasts (re-forecasts) using the Australian Bureau of Meteorology seasonal prediction system POAMA24.c are initialized on the first of each month for January 1981 to December 2013 from observed atmosphere-ocean states[4]. Ocean initial conditions are provided by the PEODAS reanalysis[27]. The quality of the PEODAS reanalyses is comparable to other operational ocean re-analyses[28]. Ensemble mean forecasts are obtained by averaging the 10 members. We refer to these hindcasts as the control forecasts. Prediction skill of ENSO using the control hindcasts is on par with other state-of-the-art coupled model seasonal forecast systems[1,4].

ENSO forecast skill is assessed using correlation of the Niño3 Index (ocean surface temperature averaged 5°N-5°S, 90°W-150°W), which captures the maximum surface temperature variability associated with ENSO. For assessment of the forecasts in 2014 we also use the Niño3.4 Index (5°N-5°S, 120°W-170°W). Forecasts are verified using the Reynolds OI-v2 surface temperature analyses[29].

Forecast Experiment

We conduct a forecast experiment by swapping the mean states of the initial conditions defined over the 2 epochs (1985-1995) and (2000-2010). Note that we have excluded the two big El Niño events (1982/83 and 1997/98) from the definition of the mean state in the earlier epoch in order to not bias the results due to the occurrence of these big events, however there is little difference in the mean state or in the impact on the forecast experiment if these two events are included in the definition of the earlier epoch mean. The mean state changes in the initial conditions are applied to the full 3-dimensional atmosphere (u, v, T, moisture, surface pressure, soil temperature and moisture) and ocean (u, v, T, and salinity) fields. Theses mean state differences are nearly identical to those derived from 2000-2013 minus 1981-1999 as depicted in Figs. 1a,b,c and Supplementary Fig. 1.

Let $X_c(0)$ represent an initial atmosphere-ocean state during the earlier epoch (1985-1995). Let $Y_c(0)$ similarly describe an observed state during the later epoch (2000-2010). The subscript *c*, for control, indicates that observed initial states are used for the control forecasts. With an overbar representing the time average over the respective epoch and a prime indicating a deviation from that mean, the initial conditions for the control forecasts in the two epochs are

$$X_c(0) = X'(0) + \overline{X}_c(0)$$

And

$$Y_c(0) = Y'(0) + \overline{Y}_c(0).$$

The initial conditions in the experiments with the swapped background climates are then

$$X_e(0) = X'(0) + \overline{Y}_c(0) = X_c(0) + \Delta$$

$$Y_e(0) = Y'(0) + \overline{X}_c(0) = Y_c(0) - \Delta$$

Here $\Delta = \overline{Y}_c - \overline{X}_c$, and noting that $\overline{X}_e = \overline{Y}_c$ and $\overline{Y}_e = \overline{X}_c$.

After swapping the initial mean states, we rerun the forecasts for the two periods and examine the experiment minus control differences. We define the forecast anomalies relative to the lead-time dependent climatology for that epoch, and we do this for control and experiment forecasts for each epoch separately.

Predictability

We assess *prediction* skill, which is the capability of the forecast system to predict observed events, by verifying forecasts against observations. We assess *predictability*, which is an inherent characteristic of the climate, using a perfect model assumption. Here we use the method of analysis of variance[30], which assumes that the predictable fraction of the total variance of the ensemble is given by

$$Var_{pred} = {Var^{*}}_{ensm} \Big/ (Var^{*}_{ensm} + Var_{sprd})$$

where

$$Var^{*}_{ensm} = Var_{ensm} - \frac{1}{N} Var_{sprd}$$

is a non-biased estimate of the variance of the ensemble mean. The variance of the ensemble spread Var_{sprd} is computed using the deviation of each of the ten members about the ensemble mean. [6].

Statistical Significance

Significance of the difference in means is assessed using a standard t-test, the difference in standard deviations using an f-test, and the differences in correlation using a t-test after applying Fischer's transform. Our null hypothesis is no difference. For the observed behavior we use a 2-sided test, but use a one sided test for the experiment-control differences. For the two 11-year epochs (1985-1995 and 2000-2010) there are 132 forecast start times. There are 228 forecast start times for 1981-1999 and 168 for 2000-2013.

References

1. Barnston, A.G., Tripett, M.K., L'Heureux, M.L., Li, S., & DeWitt, D.G. Skill of real-time seasonal ENSO model predictions during 2002-11: Is our capability increasing? *Bull. Amer. Meteor. Soc.*, **93**, 631-651 (2012).
2. Stockdale, T.N. *et al*. ECMWF seasonal forecast system 3 and its prediction of sea surface temperature. *Clim. Dynam*., **37**, 455–471 (2011).
3. Saha, S. *et al*. The NCEP Climate Forecast System Version 2 J. *Climate*, **27**, 2185–2208 (2014).
4. Zhao, M., Hendon, H.H., Alves, O. & Yin, Y. 2014: Impact of improved assimilation of temperature and salinity for coupled model seasonal forecasts. *Clim. Dynam*. **42**, 2565-2583 (2014).
5. Balmaseda, M.A., Anderson, D., & Vidard, A. Impact of Argo on analyses of the global ocean. *Geophys. Res. Lett*., **34**, L16605, doi:1(2007).
6. Hu, Z.-Z., Kumar, A., Ren, H.-L., Wang, H., L'Heureux, M. & F.-F. Jin, F.-F. Weakened interannual variability in the tropical Pacific Ocean since 2000. *J. Climate*, **26**, 2601-2613 (2013).
7. Chung, P.-H., & Li, T. Interdecadal relationship between the mean state and El Niño types. *J. Climate*, **26**, 361-379 (2013).
8. L'Heureux, M., Lee, S. & Lyon, B. Recent multidecadal strengthening of the Walker circulation across the tropical Pacific. *Nature Clim. Chng*. **3**, 571-576 (2013).
9. Xiang, B., Wang, B., & Li., T. A new paradigm for the predominance of standing Central Pacific Warming after late 1990s. *Clim. Dyn*., **41**, 327-340 (2013).
10. Kosaka, Y. & Xie, S.-P. Recent global-warming hiatus tied to equatorial Pacific surface cooling. Nature, 501, 403-407 (2013).

11. England, M.H. *et al*. Recent intensification of wind driven circulation in the Pacific and the ongoing warming hiatus. *Nature Clim. Chng*. doi: 10.101038/NCLIMATE2106 (2014).

12. Collins, M. *et al*. The impact of global warming on the tropical Pacific and El Niño. *Nature Geosc*., **3**, 391-397 (2010).

13. Wittenberg, A. T., Rosati, A., Delworth, T.L., Vecchi, G.A., & Zeng, F. ENSO modulation: Is it decadally predictable? *J. Climate*, **27**, 2667–2681 (2014).

14. McPhaden, M.J., Zebiak, S.E., & Glantz, M.H. ENSO as an integrating concept in Earth Science. Science, 314, 1740–1745 (2006).

15. Kirtman, B., & Schopf, P.S. Decadal variability in ENSO predictability and prediction. *J. Climate*, **11**, 2804-2822 (1998).

16. Tang, Y., Deng, Z., Zhou, X., Cheng, Y., & Chen, D. Interdecadal variation of ENSO predictability in multiple models. *J. Climate*, **21**, 4811-4833 (2008).

17. McPhaden, M.J., Lee, T., & McClurg, D. El Niño and its relationship to changing background conditions in the tropical Pacific Ocean. *Geophys. Res. Lett*., **38**, L15709. doi 10.1029/2011GLo48275 (2011).

18. McPhaden, M.J. A 21st century shift in the relationship between ENSO SST and warm water volume. *Geophys. Res. Lett*., **39**, L09706, doi:10.1029/2012GL051826 (2012).

19. Rodgers, K., Friedrichs, P., & Latif, M. Tropical Pacific decadal variability and its relation to decadal modulations of ENSO. *J. Climate*, **17**, 3761-3774 (2004).

20. Choi, J., An, S-I., DeWitte, B. & Hsieh, W.W. Interactive feedback between the tropical Pacific Decadal Oscillation and ENSO in a coupled general circulation model. *J. Clim*ate, **22**, 6597–6611 (2009).

21. Fedorov, A. V. & Philander. S.G. Is El Niño changing? *Science*, **288**, 1997 – 2001 (2000).

22. Zastrow, M. Stalled El Niño poised to resurge. Nature 513, doi:10.1038/513015a (2014).

23. Ogata, T., Xie, S.-P., Wittenberg, A., & Sun, D.-Z. Interdecadal amplitude modulation of El Niño-Southern Oscillation and its impact on tropical Pacific decadal variability. *J. Climate*, **26**, 7280-7297 (2013).

24. Clement, A.C., Seager, R., Cane, M.A., & Zebiak, S.E. An ocean dynamical thermostat. *J. Climate*, **9**, 2190-2196 (1996).

25. Luo, J.-J., Sasaki, W., & Masumoto, Y. Indian Ocean warming modulates Pacific climate change. *Proc. Nat., Acad. Sci. USA*, **109**, 18701-18706 (2012).

26. Power, S., Delage, F., Chung, C., Kociuba, G., & Keay, K., Robust twenty-first-century projections of El Niño and related precipitation variability. *Nature*, doi:10.1038/nature12580 (2013).

27. Yin, Y., Alves, O. & Oke, P.R. An ensemble ocean data assimilation system for seasonal prediction. *Mon. Wea. Rev.*, **139**, 786-808 (2011).

28. Xue, Y., Balmaseda, M., Boyer, T., Ferry, N., Good, S., Ishikawa, I., Kumar, A., Rienecker, M., Rosati, A., & Y. Yin, Y. A comparative analysis of upper ocean heat content variability from an ensemble of operational ocean reanalyses, *J. Climate*, DOI: http://dx.doi.org/10.1175/JCLI-D-11-00542.1 (2012)

29. Reynolds, R.W., Rayner, N.A., Smith, T.M., Stokes, D.C. & Wang, W. An improved in situ and satellite SST analysis for climate. *J. Climate*, **15**, 1609-1625 (2002).

30. Rowell, D. P., Folland, C. K., Maskell, K. & Ward, M. N. Variability of summer rainfall over tropical North Africa (1906–92): Observations and modelling. *Quart. J. Roy. Meteor. Soc.*, **121**, 669–704 (1995).

Supplementary Information is linked to the online version of the paper at www.nature.com/nature.

Acknowledgments Support for this study was provided by the Victorian Climate Initiative (VicCI). We thank D. Hudson for providing the atmosphere initial conditions, Y. Yin for providing the PEODAS ocean reanalyses, E.-P. Lim for providing technical assistance and Drs. J.-J. Luo, S.B. Power, and A Santoso for comments on an earlier draft.

Author Contributions O. A., H. H., and M.Z. conceived and designed the experiments. G.L. created the initial conditions and ran the experiments. M. Z., H. H. and G.W. conducted the analysis. H.H. wrote the first draft of the paper and all authors contributed to the revisions.

Author Information: Reprints and permissions information is available at www.nature.com/reprints. The authors declare no competing financial interests.
Correspondence and requests for materials should be addressed to hhh@bom.gov.au.

Figures

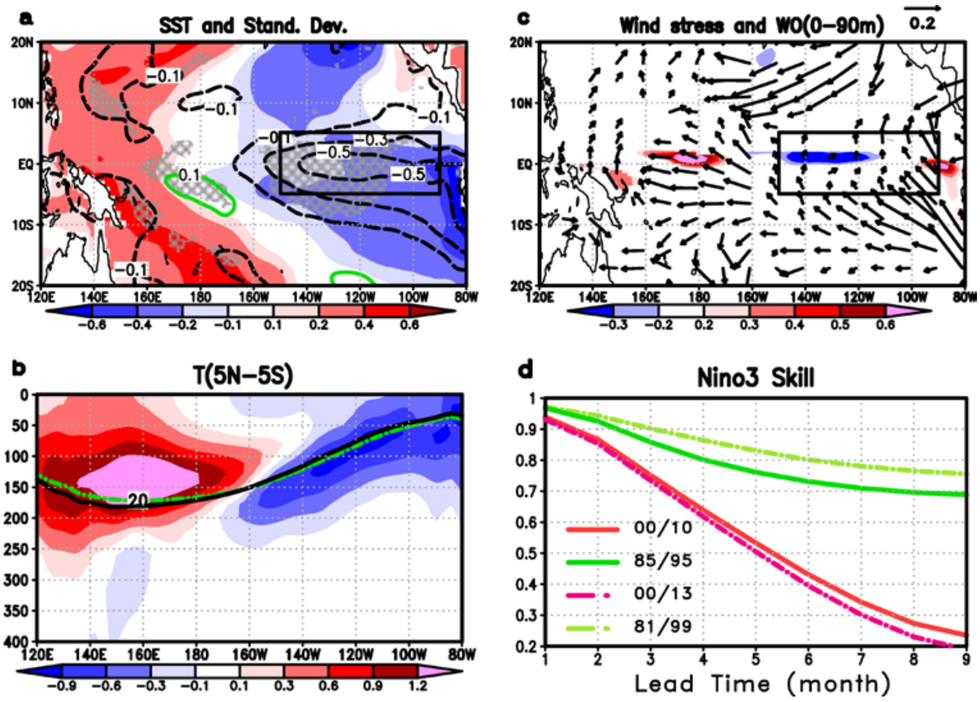

Figure 1 Epochal mean differences (2000-2013 minus 1981-1999). a: Surface temperature (shaded °C) and its monthly standard deviation (contour interval 0.2 °C with first contour at +/- 0.1, solid green for positive differences and dashed black for negative differences); **b:** temperature along equator (5°N-5°S) versus depth (shaded °C) with thermocline indicated by 20°C isotherm for later epoch (black solid) and earlier epoch (green dashed); **c:** upwelling velocity averaged 0-90 m, (shaded, units 10^{-5} m s^{-1}) and surface stress (maximum displayed vector 0.2 Nm^{-1}). **d:** prediction skill (correlation versus lead time in months) of the Niño3 index from control hindcasts initialized every month during 2000-2010 (red solid curve), 2000-2013 (red dashed curve), 1985-1995 (solid green curve) and 1981-1999 (dotted green curve). The solid black box in **a** and **c** depicts the Niño3 Index region. Mean differences in a), b) and c) are shaded and vector differences are plotted where significant for ($p<0.1$.

Significant differences (p<0.1) in standard deviation in a) are hatched. Epochal differences in correlation in d) are significant (p<0.1) at every lead time.

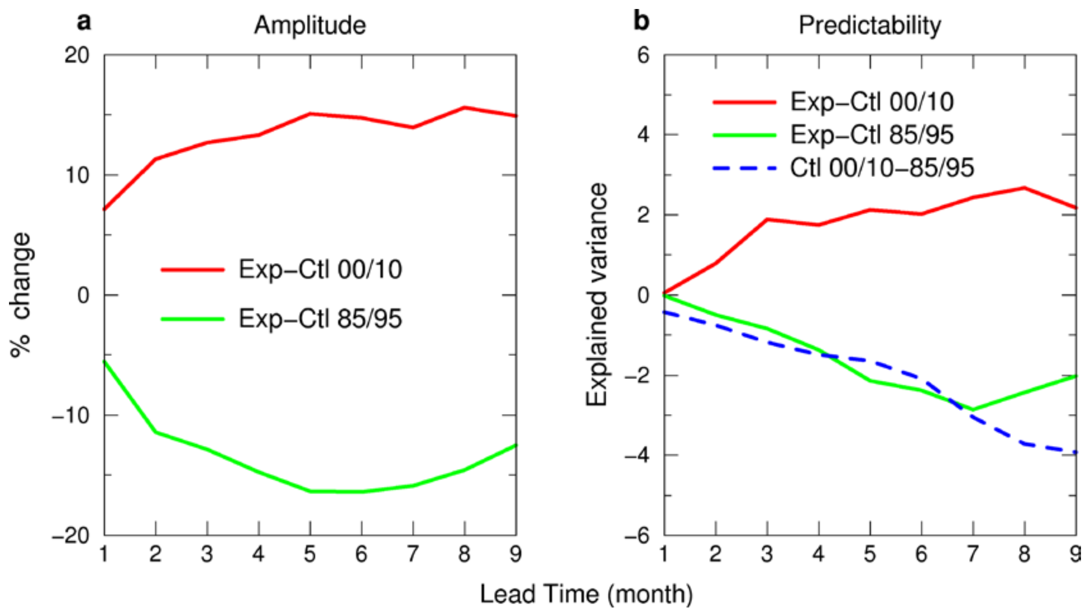

Figure 2 Changes in predicted Niño3 amplitude and predictability. a: Percentage change amplitude for the forecast experiment compared to the control for 2000-2010 period (red curve), for 1985-1995 period (solid green curve), and for 1981-1999 period (dashed-dot green curve); **b:** Differences of potential predictability (experiment minus control) for 2000-2010 (red curve) and 1985-1995 (solid green curve). Blue-dash curve denotes the difference of potential predictability for control forecasts 2000-2010 minus 1985-1995. Differences in amplitude and predictability are significant (p<0.1) for all lead times after month 1.

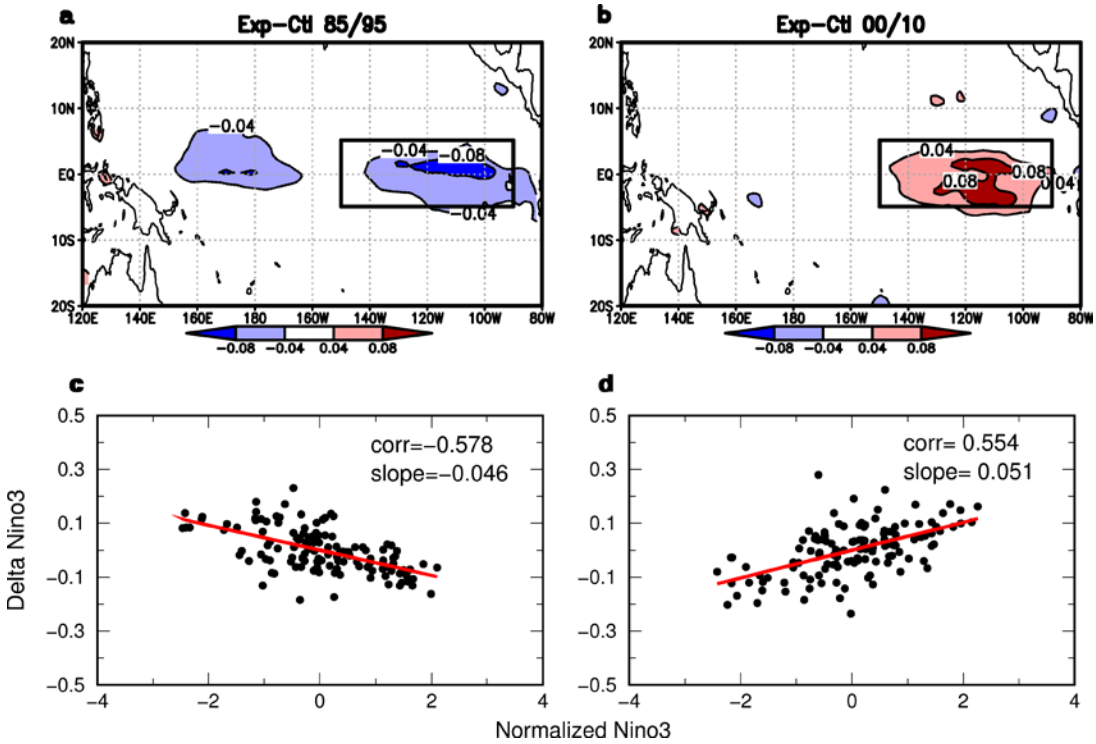

Figure 3 Experiment minus control differences in ENSO growth rate. Differences in growth rate of ENSO surface temperature anomalies computed by the regression of the difference in predicted surface temperature (experiment minus control) after 1 month onto the observed Nino3 anomaly at the initial time for **a:** 1985-1995 and **b:** 2000-2010. Differences in growth rate are shaded (unit C month-1) where significant (p<0.05, n=132). The scatter of the differences in predicted surface temperature in the Niño3 region versus the observed Nino3 anomaly at the initial time are shown for **c:** 1985-1995 and **d:** 2000-2010. The red lines in **c** and **d** are the least squares regressions onto the Niño3 Index and the slope (growth rate) has unit °C mnth^{-1}, The negative slope in **c** shows that El Niño and La Niña anomalies in the earlier epoch both weaken in response to initializing with the mean state from the later epoch. The positive slope in **d** shows that El Niño and La Niña during the later epoch both strengthen in response to the background climate from the earlier epoch. The fits (correlation) in c) and d) are significant (*p*<0.001, n=132).. The solid black box in (a) and (b) highlights the Niño3 region.

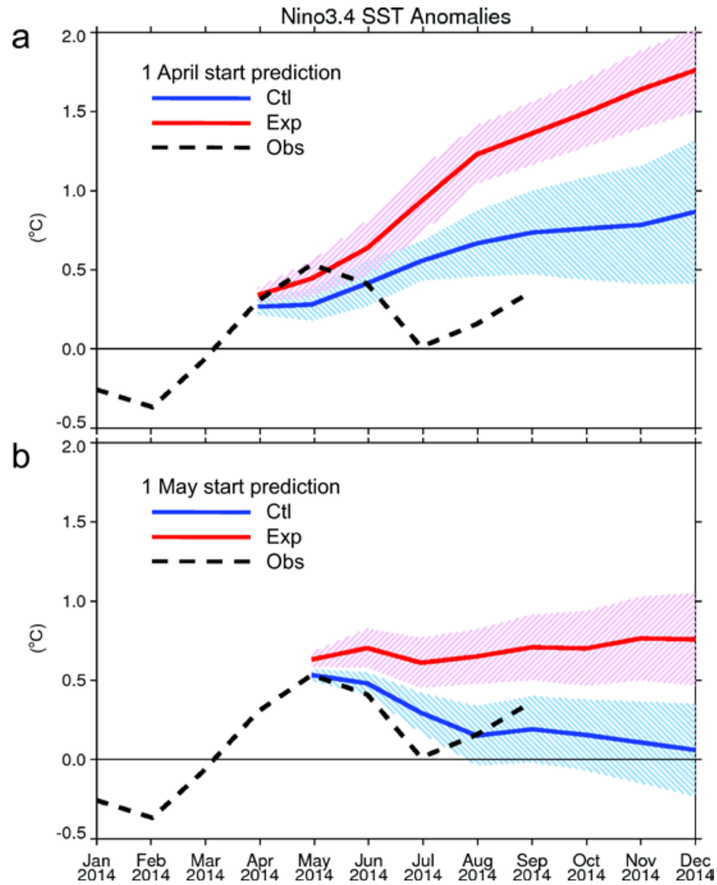

Figure 4 Predictions for El Niño 2014. Observed (dashed curve) and predicted Niño3.4 Index (5°N-5°S, 120°W-170°W) initialized on **a:** 1 April 2014 and **b:** 1 May 2014. Blue curves are operational predictions initialized with observed states and red curves are experiment predictions initialized with the 1985-1995 background climate. To be consistent with the experimental protocol, observed and predicted anomalies are formed relative to their respective 2000-2010 climatologies. Hatching is the standard deviation of the 10 member ensemble about the ensemble mean and shows that the experiment prediction from 1 April has lower spread than the operational forecast so indicating higher predictability.

Supplementary Information

Upper Ocean Heat Budget

To reveal how the atmosphere-ocean coupled processes that influence the amplitude of ENSO are affected by the changes in background climate, we consider the mixed layer heat budget (averaged 0-90 m) along the equator (averaged 5°N-5°S). To good approximation the growth of an ENSO temperature anomaly is given by[1]

$$\frac{\partial T'}{\partial t} \approx -\overline{w}\frac{\partial T'}{\partial z} - u'\partial\overline{T}/\partial x$$

Overbars denote epochal means and primes are perturbations from those means. T is the temperature averaged over the mixed layer of depth H = 90 m. W is the vertical velocity (upwelling) at base of mixed layer H and u is the zonal current averaged over depth H. The vertical temperature gradient is computed at depth H. The first term on the right hand side is referred to as the thermocline and the second term is referred to as the zonal advective feedback. We have neglected a) nonlinear terms, b) advection of the mean vertical temperature gradient by anomalous vertical velocity (the Ekman feedback term which is typically large only in the far eastern Pacific), c) advection of anomalous zonal temperature gradient by mean zonal currents, d) meridional advection, and e) surface heat fluxes and the residual terms, all of which appear to not contribute to differences in ENSO behaviour under investigation here.

We form the difference heat budget[1] for the initial month of the forecast (time 1), and use the fact that both the experiment and control forecasts start off from the same observed anomaly at time 0:

$$\Delta\frac{\partial T'}{\partial t} = \frac{T'_e(1) - T'_c(1)}{\Delta t} =$$

$$-\left[\Delta\overline{w}(1)\frac{\partial T'_c(1)}{\partial z} + \overline{w_e}(1)\Delta\frac{\partial T'(1)}{\partial z}\right] - \left[u'_c(1)\Delta\frac{\partial\overline{T}(1)}{\partial x} + \Delta u'(1)\frac{\partial\overline{T}_e(1)}{\partial x}\right] \quad (1)$$

The delta operator for means and perturbations is defined, for example, as

$$\Delta\overline{\mathrm{w}}(1) = \overline{\mathrm{w_e}}(1) - \overline{\mathrm{w_c}}(1)$$

and

$$\Delta\frac{\partial \mathrm{T}'(1)}{\partial \mathrm{z}} = \frac{\partial \mathrm{T}'_{\mathrm{e}}(1)}{\partial \mathrm{z}} - \frac{\partial \mathrm{T}'_{\mathrm{c}}(1)}{\partial \mathrm{z}}$$

The left hand side of (1) is the total difference in tendency in month 1 as a result of imposing the change in mean state at the initial time. The thermocline feedback (first set of brackets on the right hand side of (1)) is composed of the difference in mean vertical velocity acting on the perturbation vertical temperature gradient and the mean vertical velocity acting on the induced change in perturbation vertical temperature gradient. The zonal advective feedback (second set of brackets on right hand side of (1)) is composed of the anomalous zonal current acting on the difference in mean zonal temperature gradient, and the induced change in anomalous zonal current acting on the mean zonal gradient.

To highlight how ENSO anomalies react to the imposed change in mean state, we form a composite difference heat budget by regressing all terms in (1) onto the normalized observed Niño3 anomaly at the initial forecast time, recognizing that both the control and experiment forecasts are initialized with the same anomalies. The regression of the first term in each bracket of (1) reveals the direct response due to the imposed change in the background climate, while the second term reveals the result of a change in the anomaly during the forecast due to the imposed change in background climate.

Supplementary References

1. DiNezio, P.N., Kirtman, B.P., Clement, A.C., Lee, S.K., Vecchi, G.A. & Wittenberg, A. Mean climate controls on the simulated response of ENSO to increasing greenhouse gases. *J. Climate*, **25**, 7399-7420 (2012).
2. Kalnay, E. *et al*. The NCEP/NCAR Reanalysis 40-year Project. *Bull. Amer. Meteor. Soc*., **77**, 437-471 (1996).
3. Xie, P., & Arkin, P.A. Global precipitation: A 17-year monthly analysis based on gauge observations, satellite estimates, and numerical model outputs. *Bull. Amer. Meteor. Soc*., **78**, 2539 - 2558 (1997).

Supplementary Figures

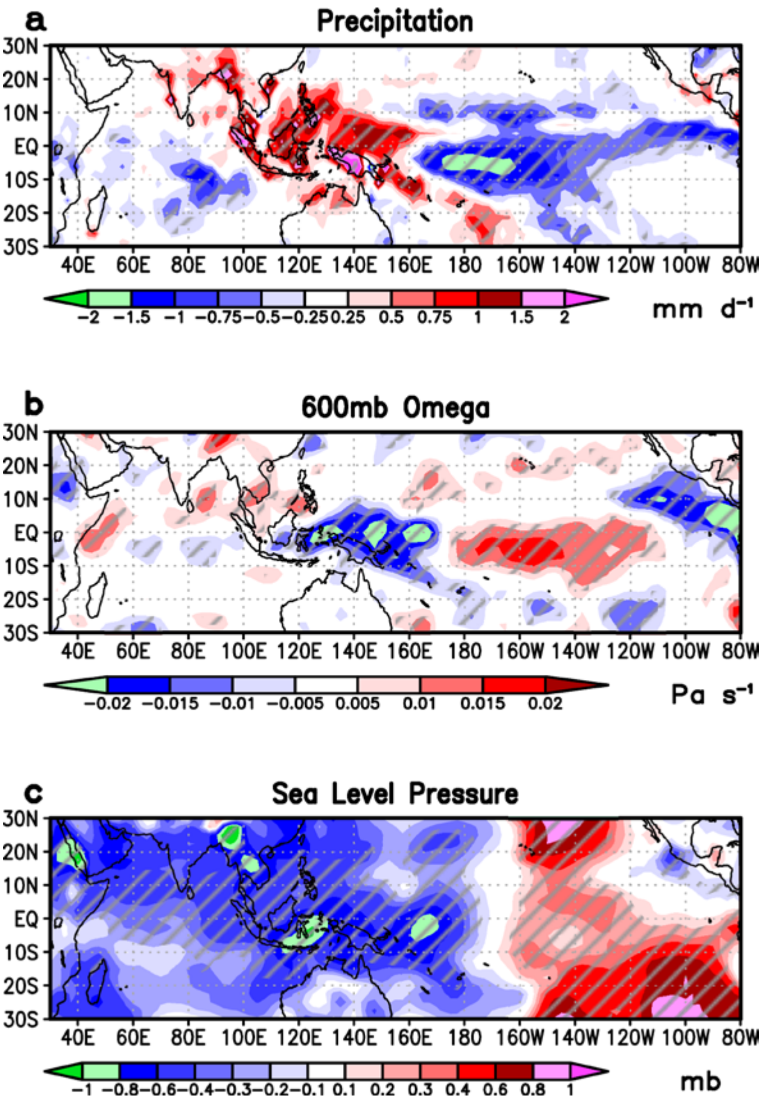

Supplementary Fig. 1: Epochal mean differences (2000-2013) minus (1981-1999) for **a:** CMAP rainfall[37], and **b**: pressure vertical velocity at 600 hPa and **c**: sea level pressure from NCEP reanalyses[33]. Significant difference are hatched (p<0.1). Data acquired from NOAA/ESRL Physical Sciences Division, Boulder Colorado http://www.esrl.noaa.gov/psd

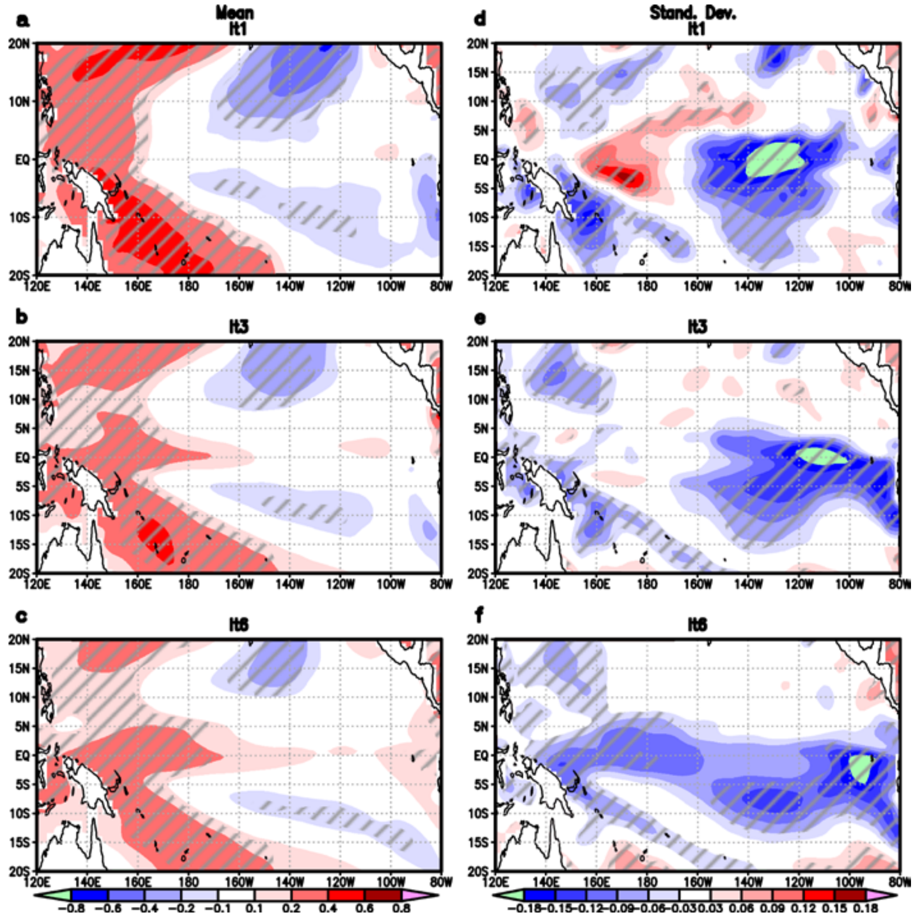

Supplementary Figure 2: Difference in mean SST from control forecasts (2000-2010 minus 1985-1995) at lead time **a**: 1, **b**: 3 and **c**: 6 months. (**d-f**) As is **(a-c**) except for difference in standard deviation. Units are °C. Significant differences (p<0.1) are hatched.

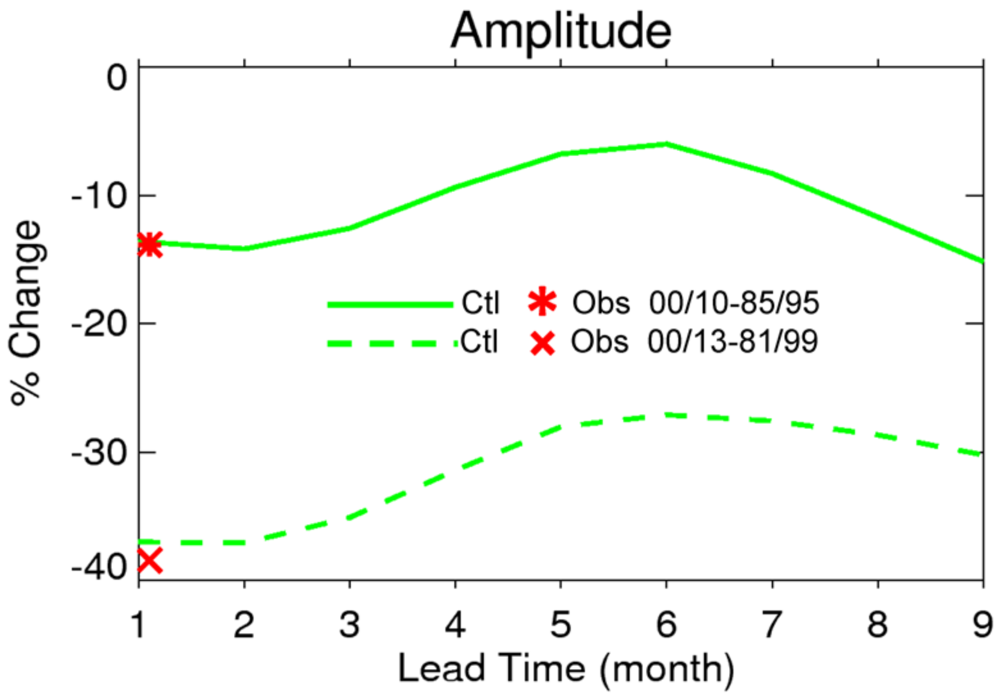

Supplementary Fig. 3: Percentage change in predicted amplitude of Niño3 Index in control forecasts 2000-2010 compared to 1985-1995 (solid green curve) and 2000-2013 compared to to 1981-1999 (dash green curve). Asterisks indicate the percentage change of observed Niño3 amplitude for 2000-2010 compared to 1985-1995 (bold asterisk) and 2000-2013 compared to 1981-1999 (light asterisk). Observed and forecast difference in amplitude are all significant (p<0.1, n=132)

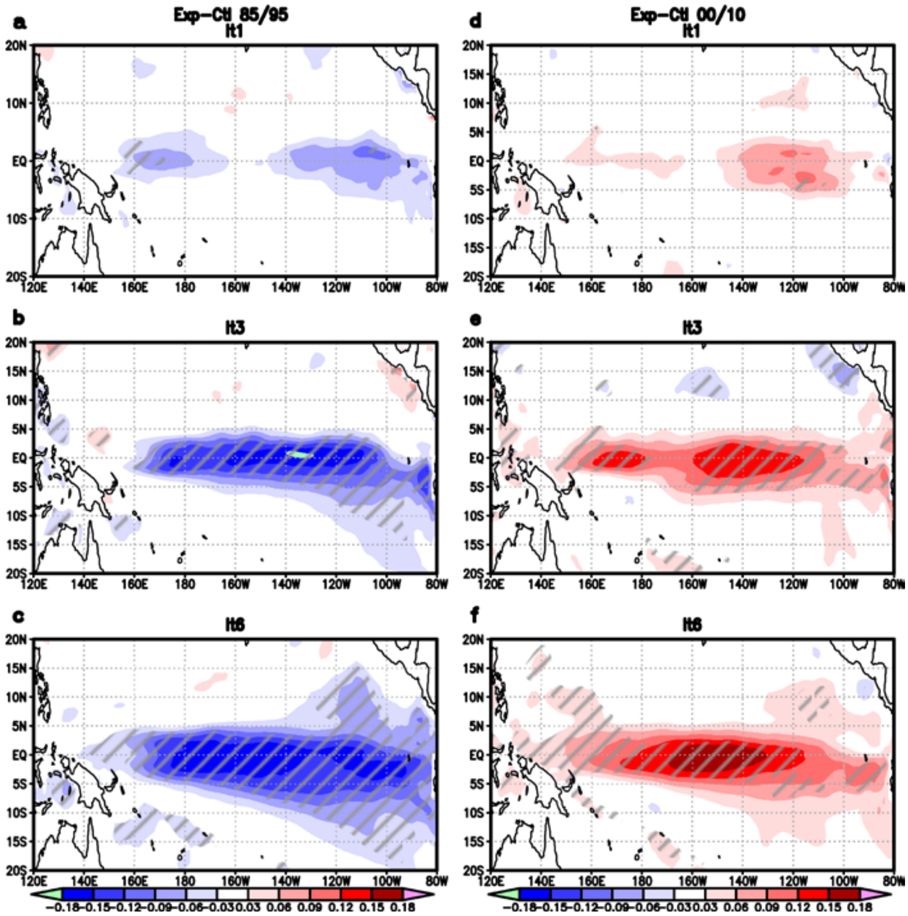

Supplementary Fig. 4: Differences in standard deviation of SST (experiment minus control) for (left) 1985-1995, and (right) 2000-2010 for lead times 1 monht (a,d), 3 month (b,e) and 6 months (c,f).   . Significant differences ($p<0.1$, $n=132$) are hatched.

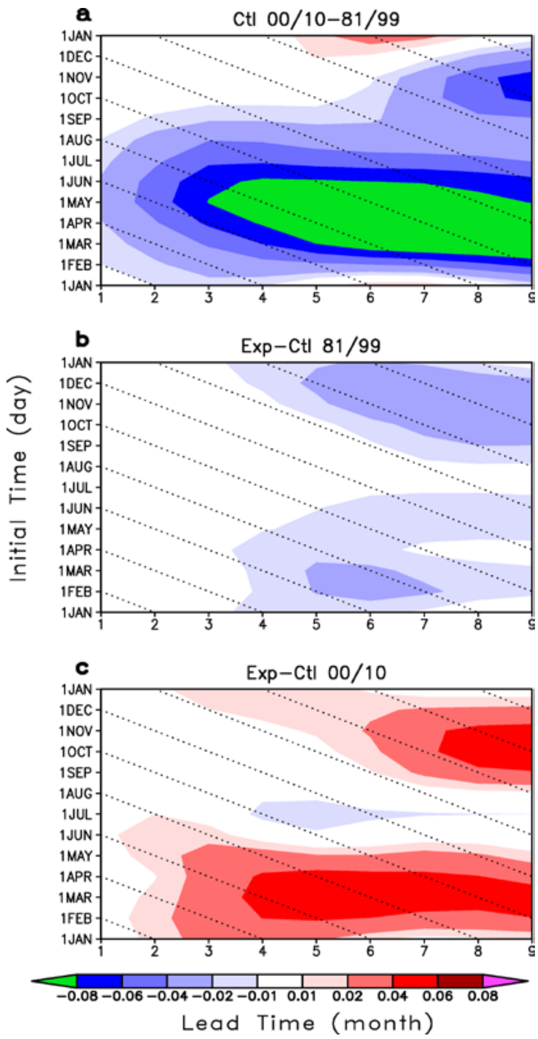

Supplementary Fig. 5: Differences in potential predictability (explained variance) of Niño3 Index for **a**: control forecasts 2000-2010 minus 1981-1999; **b**: experiment minus control forecasts for 1981-1999 and **c:** experiment minus control forecasts for 2000-2010. Difference in predictability is shown as a function of forecast start month (y-axis) and lead time (x axis). Dotted sloping lines indicate a constant verification month but at varying lead time.

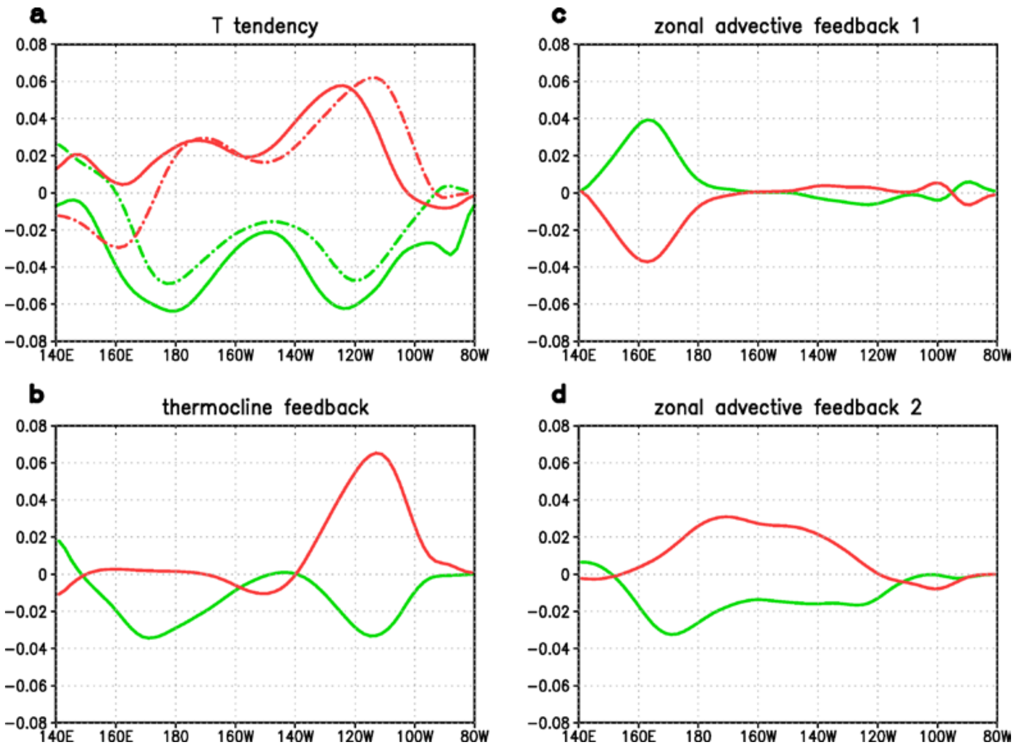

Supplementary Fig. 6: Differences in predicted upper ocean temperature tendency (experiment minus control) at month 1 averaged in latitude (5°N-5°S) and over depth (0-90 m). **a**: Differences in total temperature tendency (solid curves) and tendency approximated by the sum of the three components shown in panels (**b,c,d**) (dot-dashed curves); **b:** Difference in thermocline feedback tendency due to mean change in background upwelling; **c**: Difference in zonal advective tendency due to mean change in background zonal temperature gradient; and **d**: Difference in zonal advective tendency due to the induced change in zonal current anomalies during forecast. The tendency differences (experiment minus control) are computed as the respective tendency differences from month 1 of the experiment and control forecasts regressed onto the observed normalized Niño3 Index anomaly at the initial time. Scale for tendency differences has units °C mnth^{-1}. Red curves are experiment minus control forecasts for 2000-2010 and green curves for 1985-1995.

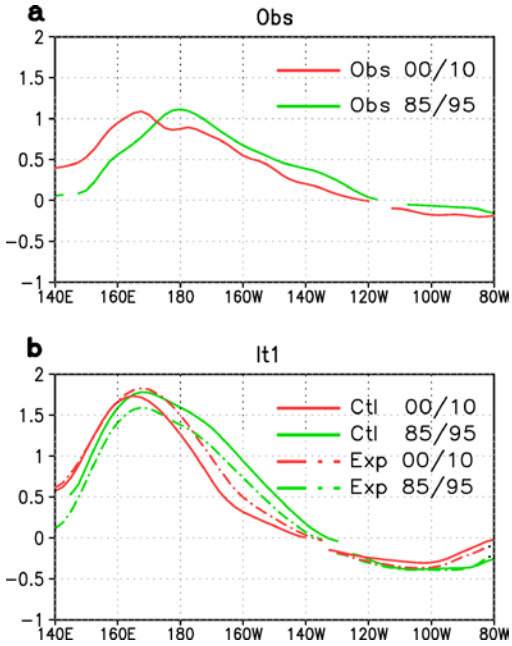

Supplementary Fig. 7: Regression of normalized Niño3 index onto zonal surface wind anomalies (5°N-5°S) **a**: for observations, and **b**: for control (solid curves) and experiment (dot-dash curves) forecasts at lead time 1 month. The red curves denote 2000-2010 period and green curves denote 1985-1995 period. Curves are only plotted where regression is significant ($p<0.1$).